European Commission

JRC TECHNICAL REPORTS

Energy dependant neutron multiplicity in ^{235}U(n,f)

Göök A., Hambsch F.-J., Oberstedt S., Vidali M.

Public

2017

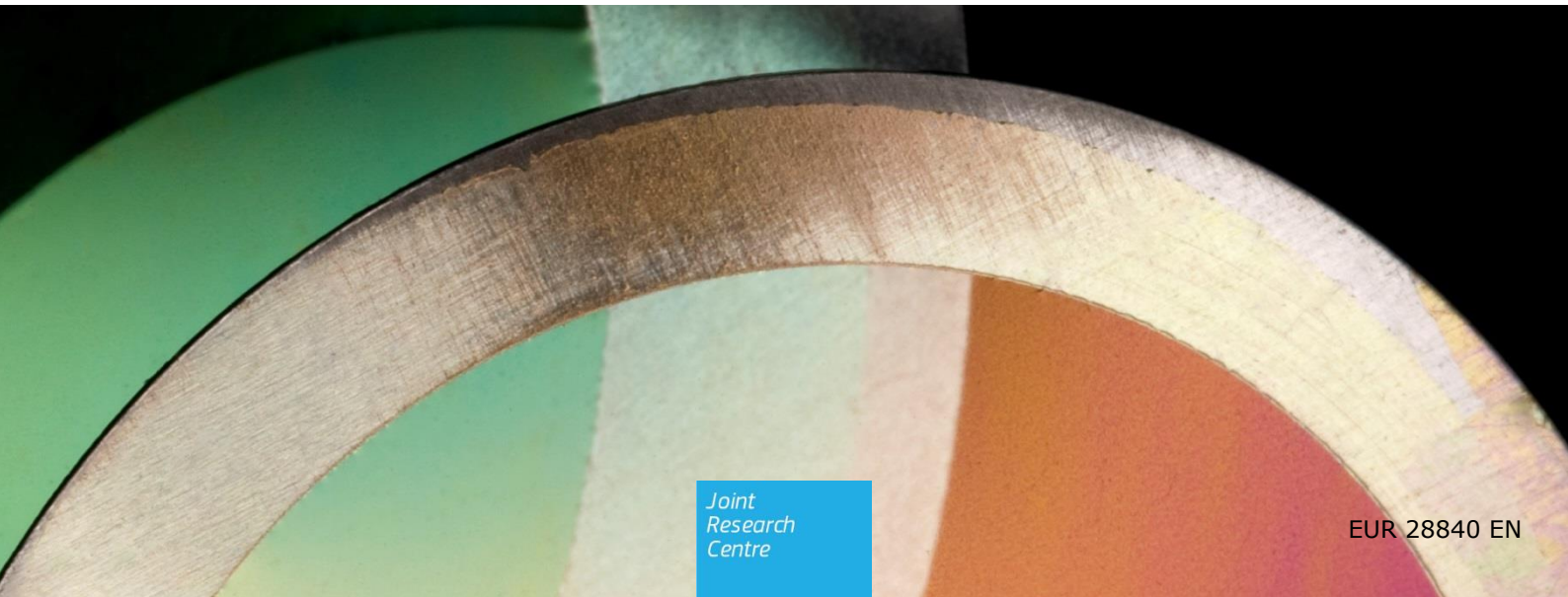

Joint Research Centre

EUR 28840 EN

Contact information
Name: Stephan Oberstedt
Address: European Commission, Joint Research Centre, Retieseweg 111, 2440 Geel, Belgium
Email: Stephan.OBERSTEDT@ec.europa.eu
Tel.: +32-14-571361

JRC Science Hub
https://ec.europa.eu/jrc

JRC108456

PDF ISBN 978-92-79-74380-1 ISSN 1831-9424 doi:10.2760/481835

Luxembourg: Publications Office of the European Union, 2017

How to cite this report: Göök A., Hambsch F.-J., Oberstedt S., Vidali M., *Energy dependant neutron multiplicity in ^{235}U(n,f)*, EUR 28840 EN, Publications Office of the European Union, Luxembourg, 2017, ISBN 978-92-79-74380-1, doi10.2760/481835, PUBSY No. 108456

Title Energy dependant neutron multiplicity in ^{235}U(n,f)

Abstract
Experimental activities at JRC-Geel on prompt-fission-neutron (PFN) emission in response to OECD/NEA nuclear data requests are presented in this report. Specifically, investigations of PFN emission from the reaction ^{235}U(n,f) in the region of the resolved resonances are presented. The experiment employs a scintillation detector array for neutron detection, while fission fragment properties are determined via the double kinetic energy technique using a position sensitive twin ionization chamber. This setup allows us to study several correlations between properties of neutron and fission fragments simultaneously. Results on PFN correlations with fission fragment properties from the present study differ significantly from earlier studies on this reaction, induced by thermal neutrons.

Contents

Acknowledgements

The authors would like to acknowledge the GELINA operators team for providing the neutron beam. Wouter Geerts and Cedric Bonaldi are acknowledged for their help in the set-up of the experiment and design of the SCINTIA detector frame.

Authors

Alf Göök, Franz-Josef Hambsch, Stephan Oberstedt, Marzio Vidali

Joint Research Centre - JRC

Directorate G – Nuclear Safety & Security

Unit G.2 - Standards for Nuclear Safety, Security & Safeguards

Retieseweg 111

B-2440 Geel/Belgium

Abstract

Experimental activities at JRC-Geel on prompt-fission-neutron (PFN) emission in response to OECD/NEA nuclear data requests are presented in this report. Specifically, investigations of PFN emission from the reaction ^{235}U(n,f) in the region of the resolved resonances are presented. The experiment employs a scintillation detector array for neutron detection, while fission fragment properties are determined via the double kinetic energy technique using a position sensitive twin ionization chamber. This setup allows us to study several correlations between properties of neutron and fission fragments simultaneously. Results on PFN correlations with fission fragment properties from the present study differ significantly from earlier studies on this reaction, induced by thermal neutrons.

1 Introduction

Experimental investigations of prompt fission neutrons and fission fragment properties in resonance neutron induced fission on ^{235}U have been performed at the GELINA facility of the JRC-Geel. Improved knowledge of the properties of prompt fission neutrons (PFN), their multiplicities, as well as their energy and angular distributions are not only of interest for questions related to the neutron emission itself, but also to questions relevant to the formation of the fission fragments, the sharing of excitation energy among them and the time scale of the process.

In recent years large efforts have been put into the modelling of PFN emission in fission (Capote et al., 2016). One of the major driving forces behind these efforts is develop tools for improved evaluations of nuclear data on prompt fission neutron spectra (PFNS) in neutron induced fission. For many applications in nuclear science and technology the PFNS plays an important role. Particularly, the use of neutron transport codes to accurately predict nuclear criticality relies heavily on accurate nuclear data, and the PFNS data can have a very strong impact on the results. For example, it has been demonstrated that for certain ^{239}Pu solution thermal-critical assemblies with high neutron leakage, a change in average neutron energy of 1-2 % (corresponding to evaluated PFNS generated by different evaluators) the variation in the obtained k_{eff} can approach 1000 pcm (De Saint Jean and McKnight, 2014 and Peneliau et al., 2014). The efforts to model PFN emission in fission are quite successful in both consistency between different approaches and reproducing available experimental data. However, in the case of ^{235}U(n,f) difficulties have been encountered (Lemaire et al, 2005), especially regarding the dependency of the average number of neutrons emitted per fission on the fragment total kinetic energy (TKE). Possible deficiencies in the available experimental data have been pointed out by Kornilov (Kornilov et al., 2015). Correlated PFN and fission fragment data are used in the development of the models to verify theoretical assumptions. As the models require accurate experimental data for validation it is of importance to revisit PFN correlations with fission fragment properties in ^{235}U(n,f) experimentally.

In resonance neutron induced fission, the variation of the average number of neutrons emitted per fission $\bar{\nu}$ with the incident neutron energy, has remained an open question. Previous measurements have established that $\bar{\nu}$ shows fluctuations from resonance to resonance. However, a satisfying explanation for this behaviour is lacking as no correlation between $\bar{\nu}$ with resonance spin nor fission width has been established. Fluctuating $\bar{\nu}$ in the resonance region can have strong impact on applications as shown by recent efforts to improve the ^{235}U nuclear data evaluation (Pigni, 2016). With changes in thermal neutron constants as well as PFNS it was necessary to take into account fluctuations of $\bar{\nu}$ below 100 eV in order to restore good performance for k_{eff} for thermal solution assemblies and high-leakage-solution benchmarks.

2 Experimental setup

The experiment has been performed at the GELINA facility of the JRC-Geel site. The experimental setup, illustrated in **Figure 1**, is located at a distance of 9.2 m from the GELINA neutron source. Fission fragments are detected in a position sensitive twin ionization chamber (IC). This detector has been developed at JRC-Geel, and is described in detail elsewhere (Göök et al., 2016). Essentially, it is a standard twin Frisch grid ionization chamber with the anode plates replaced by position sensitive readouts. It is capable of determining the fission axis orientation in space with a resolution of 7°, simultaneously with the fission fragment masses and energies.

Figure 1. (Left) Schematic drawing (not to scale) of the experimental setup installed at flightpath 17-10m at the Gelina facility. The neutron beam enters from the top of the drawing and hit the 235U-target located in the centre of the ionization chamber (IC). (Right) 3-dimensional representation of the detector setup, neutron detector scintillator-cells are coloured red. For the sake of illustration structural parts of the detector setup are not drawn.

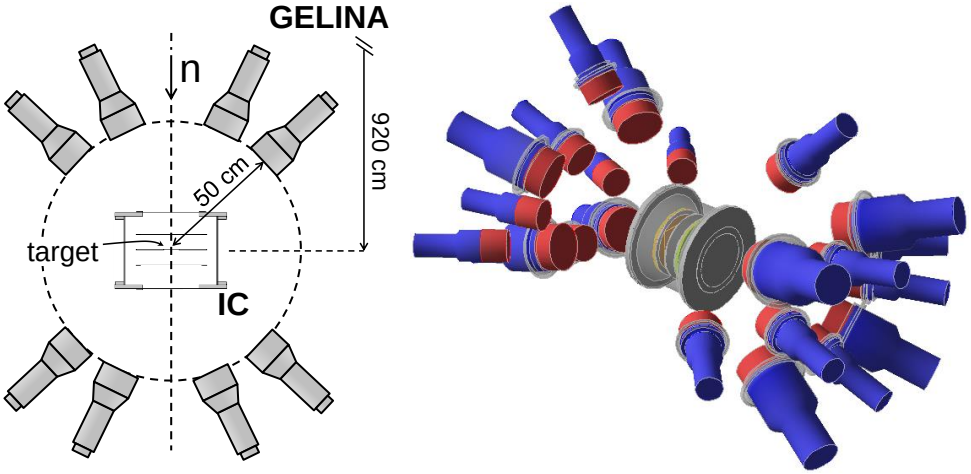

Neutrons are detected in an array of proton recoil scintillators. The array consists of 19 NE213 equivalent BC-501 liquid scintillators, 3 p-terphenyl and 1 stilbene crystal scintillators. The detectors are placed in a quasi-spherical geometry around the centre of the ^{235}U-target at distance of about 50 cm. The actual position of the detectors relative to the IC has been determined with high precision using a ROMER arm measuring device ([1]).

The data acquisition is based on wave-form digitizers, sampling the detector signals at 400 MSample/s with 14-bit resolution. A fission trigger derived from the charge induced on the central cathode of the IC, triggers the data acquisition. For every fission-trigger digital wave-forms of all neutron detectors as well as the IC's electrodes are stored on disk, together with time-stamp information, for off-line analysis. The time stamp is reset by every beam pulse from the GELINA and used to determine the incident neutron time-of-flight.

([1]) http://www.hexagonmi.com/products/portable-measuring-arms/romer-absolute-arm

3 Data analysis

3.1 Treatment of neutron detector data

Events in the scintillation detectors corresponding to neutrons are selected by means of pulse-shape discrimination (PSD). The PFN energy is measured by means of the time-of-flight technique, with a resolution of about 1 ns (FWHM). In addition to PFNs, the fission process is accompanied by prompt fission γ-rays, which might be detected in the scintillation detectors as well. Most of the γ-ray emission takes place within a few ns after the instant of fission. Therefore, the range of high-energy neutrons is most sensitive to false events induced by γ-rays. The PSD is not able to give a clean discrimination between γ-rays and neutron events for pulse heights corresponding to a proton recoil energy smaller than about 1 MeV. In order to reduce the background caused by the γ-ray emission a dynamic light-threshold (Kornilov et al., 2015) is applied.

Each detector in the SCINTIA array has been characterized using the PFNs from ^{252}Cf(sf), with experimental setup and procedures as described in(Kornilov et al.,2009). To correct for the energy dependent detection efficiency and multiple scattering of neutrons on the surrounding materials, the setup is modelled with GEANT4. The simulation uses experimentally determined proton light output functions, for other recoil-particle species literature data are used (Verbinski et al., 1986 and Tajik et al., 2013). The Monte-Carlo model has been validated against the standard PFN spectrum (Mannhart, 1986) from the spontaneous fission decay of ^{252}Cf.

3.2 Determination of fission fragment properties

The fission fragment mass and kinetic energy before neutron emission is obtained by means of the well-established double kinetic energy (2E) technique, which relates the masses $m_{1,2}^*$ and energies $E_{1,2}^*$ before neutron emission in a binary fission event according to

$$m_{1,2}^* = m_{cn}\frac{E_{2,1}^*}{E_1^* + E_2^*} \tag{1}$$

where m_{cn} is the mass of the compound nucleus undergoing fission. Under the assumption of isotropic neutron emission from fully accelerated fragments, the energies before neutron emission E^* are related to the energies after neutron emission E according to

$$E^* = E\frac{m^*}{m^* - \nu} \tag{2}$$

where ν is the number of neutrons emitted by the fragment. In the analysis ν is approximated by $\bar{\nu}(m^*,\mathrm{TKE})$, the average number of emitted neutrons for a specified mass and TKE. The dependence of $\bar{\nu}$ on mass and TKE can only be derived from the data once the 2E-analysis is completed. As initial assumption we have used the evaluated data on $\bar{\nu}(m^*)$ from Wahl (Wahl, 1988) and the parameterization

$$\bar{\nu}(m^*,TKE) = \bar{\nu}(m^*) + \frac{\bar{\nu}(m^*)}{\bar{\nu}(m^*) + \bar{\nu}(m_{cn} - m^*)}\Delta_{TKE},$$

$$\Delta_{TKE} = \frac{\overline{TKE}(m^*) - TKE}{E_{sep}} \tag{3}$$

where $E_{sep} = 8.6$ MeV/n is the average energy necessary to emit a neutron (Nifenecker, 1973). The analysis was later repeated using the results on $\bar{\nu}(m^*)$ and $E_{sep} = 8.51$ MeV/n derived from the data. No significant changes in the results were observed between the two analyses, therefore further iterations were not made. In the 2E-technique the main contribution to the mass resolution is the neutron evaporation, since Eq. (2) only holds

on average. In this work the mass resolution is 4-5 u (FWHM), determined by comparing the measured thermal mass yield to high resolution data (Geltenbort et al., 1986). This mass resolution is close to what can be expected considering only the contribution from the neutron evaporation (Terrell, 1962). For events where neutrons and fission fragments are detected in coincidence, an additional correction (Gavron, 1974) for the recoil energy imparted to the fragment is added to Eq.(2).

4 Experimental results on PFN and FF correlations

All results on correlations between fission fragment properties and PFN properties presented in this section are from the selected incident neutron energy range [0.3~eV,~45~keV]. Some of the results presented in this section and originating from a subset of the data from the present experiment, has been reported upon earlier. The main difference between results reported by us in that publication (Göök et al., 2017) and reported here is, aside from the improved statistical accuracy, that the absolute neutron detection efficiency was re-evaluated. This effectively raised the mean total neutron multiplicity from 2.3 to 2.4 neutrons/fission.

In **Figure 2** the ^{235}U(n,f) prompt fission neutron spectrum (PFNS) observed in this study, when selecting the incident neutron energy range [0.3 eV, 45 keV], is compared to the spectrum from cold neutron induced fission determined by Kornilov et al. (Kornilov et al., 2010). The two spectra are in quite close agreement, although the spectrum observed in the resonance region is slightly softer.

Figure 2. The prompt fission neutron spectrum (PFNS) in the laboratory frame. Data from this study is compared to data on cold-neutron induced fission from Kornilov et al. . (Kornilov et al., 2010) as well as a recent evaluation of the thermal neutron induced PFNS (Trkov et al., 2015). (Left) The PFNS in logarithmic scale. (Right) The PFNS represented as a ratio to a Maxellian with a temperature of 1.32 MeV.

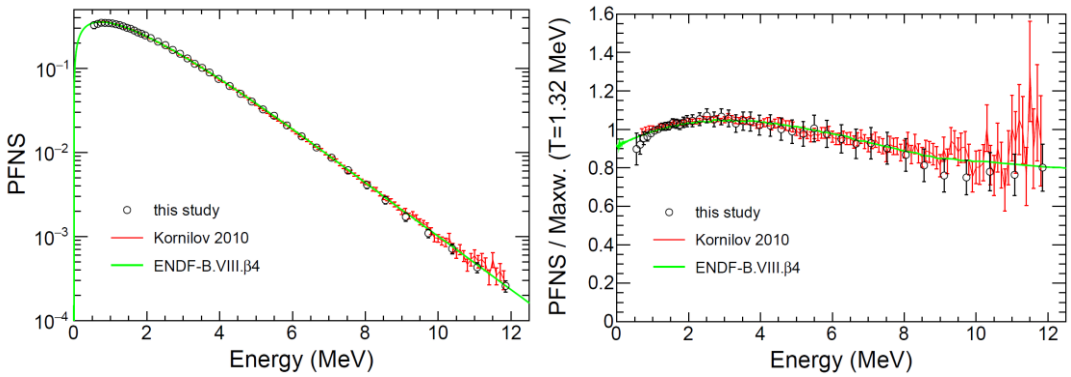

4.1 Prompt fission neutron angular distributions in the laboratory frame

Most model calculations of the properties of PFNs are based on the assumption that the neutrons are emitted from the fragments after they have reached their terminal velocity. However, theoretical arguments have been raised asserting that at least a fraction of the neutrons are emitted during the scission process (Rizea and Carjan, 2013) and/or during the acceleration of the fragments (Eismont, 1965). A large number of experiments have been devoted to investigate the source of prompt neutrons in detail. However, considering the variation of experimental results it is difficult to draw definitive conclusions. The experimental method used here, as well as in many earlier studies (Nishio et al., 1998, Vorobyev et al., 2010 and Maslin et al., 1967) of PFN emission in ^{235}U(n,f), assumes that the neutrons are emitted from the fully accelerated fragment. Hence, it is of great importance to investigate to what extent the experimental data support this assumption. In order to do so, we follow a procedure similar to that of Vorobyev et al., 2009. The energy-angle distribution of neutrons emitted from moving fragments when observed in the laboratory frame is

$$N(E_n,\theta) = N_L(\eta_L,\vartheta_L)\sqrt{\frac{E_n}{\eta_L}} + N_H(\eta_H,\vartheta_H)\sqrt{\frac{E_n}{\eta_H}}\,, \qquad (4)$$

where $N_{L,H}(\eta_{L,H}, \vartheta_{L,H})$ are the center-of-mass (c.m.) energy-angle distributions of neutrons from the light and heavy fragments, respectively. The neutron energies in the c.m. frame $\eta_{L,H}$ can be derived from experimental observables in the laboratory frame; light (L) and heavy (H) fragment energies $E_{L,H}$ and masses $m_{L,H}$, neutron energy E_n and angle θ between the detected neutron's and the fragment's directions of motion

$$\eta_{L,H} = E_n + E_{L,H}\frac{m}{m_{L,H}} - 2\sqrt{E_n E_{L,H}\frac{m}{m_{L,H}}}\cos\theta, \quad (5)$$

where m is the mass of the neutron. For the purpose of the model a single fragmentation is used, with $E_L\frac{m}{m_L} = (1.02 \pm 0.01)$ MeV and $E_H\frac{m}{m_H} = (0.491 \pm 0.01)$ MeV taken as averages from the experimental data. Under assumption of isotropic emission from the fully accelerated fragments, only the neutron spectra in the c.m. frame are unknown. They are determined from the experimental data by selecting small angles in the laboratory frame, where the contribution of neutrons from the complementary fragment is the smallest. Neutrons detected at angles smaller than 12° relative to the motion of the light and heavy fission fragments are selected. The observed laboratory spectra for these selections are transformed into the c.m. frame of the respective fragment and corrected for the small contribution of neutrons from the complementary fragment; the result is displayed in **Figure 3**. Each of the spectra has been fitted with a linear superposition of a Maxwellian and a Watt spectrum shape, represented by the full black lines. The fitted shapes are then used to calculate the spectrum as a function of the angle between the light fission fragment direction and the detected neutron, according to Eq. (4).

Figure 3. The c.m. neutron energy spectra of light and heavy fission fragment groups.

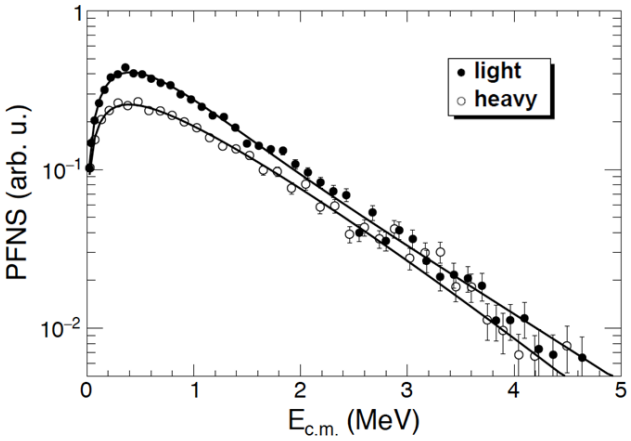

The result of the calculation is presented as a contour plot in **Figure 4**. As can be seen, the contour lines of the model do follow the contour lines of the experimental data quite well. In **Figure 5** the zeroth (Left) and the first (Right) moments of the calculated and experimentally observed spectra as a function of $\cos\theta$ are compared. The agreement is fair, although an underestimation of the experimental data is evident. At 90° the underestimation amounts to about 25 % of the neutron yield. The total neutron yield is underestimated by 2.5 % by the model. It is also evident that the average neutron energy at increasing angles with the fission axis is underestimated by the model. The underestimation is largest at 90°, where it amounts to about 6 %. The description of the experimental data could be improved by assuming a small anisotropy in the c.m. frame (Vorobyev, 2009). However, we did not include an anisotropy term in the evaluation of the laboratory data as the angular distribution observed in the c.m. frame does not allow for this degree of freedom, see Sect 4.2.1. Considering the simplifying assumptions made in the model the description must be considered good. In order to investigate the sensitivity of the analysis to neutron sources other than fully accelerated fragments

further work is required. For the present, we conclude that the assumption of isotropic emission from fully accelerated fragments is not contradicted by the experimental data, although contributions from other mechanisms of neutron emission cannot be excluded.

Figure 4. The laboratory energy-angle distribution of prompt neutrons. The experimental data are represented by a contour-plot with black contour lines on top of a color-coded scatter-plot. The red contour lines represent the model calculation according to Eq. (4) with adjusted parameters, see text for details..

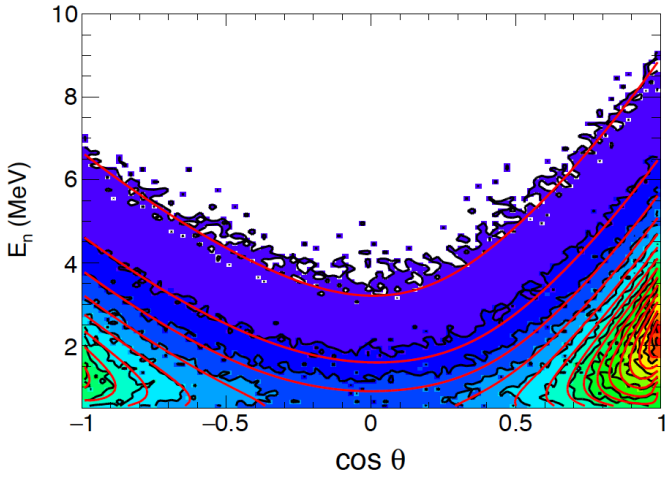

Figure 5. (Left) Projection of the data in **Figure 4** onto $\cos\theta$. (Right) The Average neutron energy as a function of $\cos\theta$. The red lines represent the result of the model calculation.

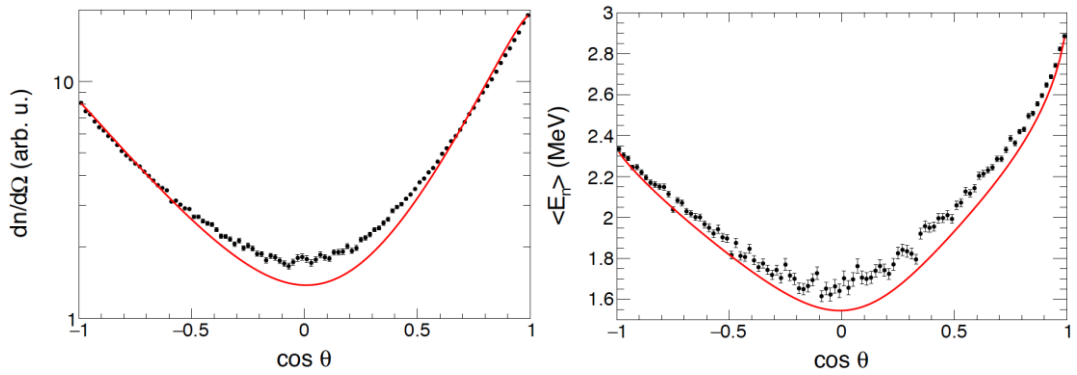

4.2 Experimental results in the fission fragment rest-frame

The complete experimental determination of all relevant kinematic parameters allows the transformation from the laboratory frame of reference into the rest frame of the fully accelerated fission fragments. This transformation is, however, complicated by the fact that for each laboratory angle only the sum of contributions from the two fission fragments is observed. Thus, an unknown contribution must first be subtracted from any observed distribution. Fortunately, the contribution of neutrons emitted from the fragment flying away from the neutron detector is small. Therefore, in a first approximation it is assumed that all neutrons that are detected with a c.m. angle $\theta_{\mathrm{c.m.}}$ smaller than 90° originate from the fragment directed towards the neutron detector. The resulting distribution is then used to calculate the disturbing component from the complementary fragment. The magnitude of the correction as a function of fission fragment mass is shown in **Figure 6**.

Figure 6. Fission neutron yield for $\theta_{\text{c.m.}} < 90°$ as a function of the fission fragment mass. The red points represent the calculated contribution of neutrons from the complementary fission fragment.

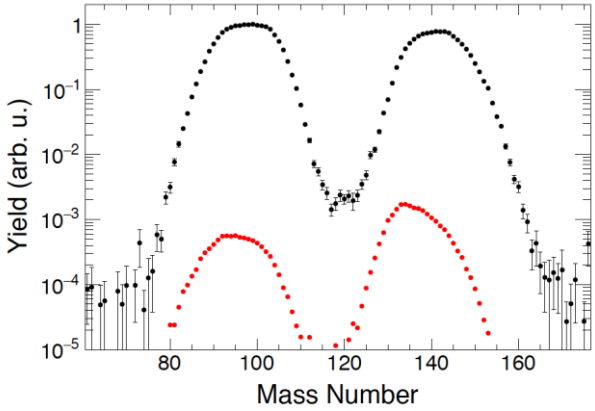

4.2.1 Angular distribution

Using the procedures discussed above the angular distribution of prompt neutrons in the rest frame of the fully accelerated fragments has been determined. **Figure 7** shows the angular distribution integrated over all c.m. neutron energies and all fission configurations, i.e. no selection in mass or TKE has been made. The result has been fitted with a second order Legendre polynomial. Obviously, the result supports isotropic emission in the c.m.-frame. This does, however, not exclude emission from neutron sources other than fully-accelerated fragments due to the selection of events with $\theta_{\text{c.m.}} < 90°$. The selection implies that events with laboratory neutron energies smaller than the fragment energy per nucleon are rejected in the analysis.

Figure 7. Angular distribution of prompt neutrons in the c.m. frame integrated over all neutron energies and fission configurations.

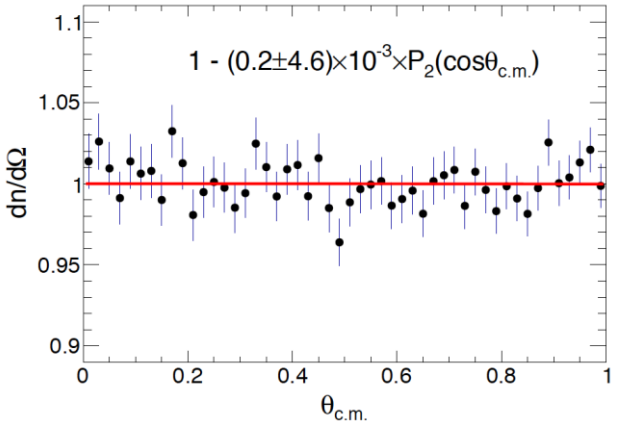

4.2.2 Average neutron multiplicity

The average neutron multiplicity as a function of the fragment mass is shown on the left hand side of **Figure 8**. For comparison, experimental data from the literature (Nishio et al., 1998 and Vorobyev et al., 2010) as well as evaluated data (Wahl, 1988) are also shown in the figure. The general sawtooth like shape is reproduced in this work, however

the minima around mass number 80 for the light fragments and 130 for the heavy fragments appear more pronounced in the present data. The average neutron multiplicity per fission is shown as a function of the heavy fragment mass on the right hand side of **Figure 8**, a pronounced minimum is observed close to heavy fragment mass 132. The shape of the present data agrees very well with the data from Maslin et al, 1967.

Figure 8. (Left) The average neutron multiplicity per fragment as a function of the fragment mass from this study compared to data from Refs. [20, 21] and the evaluation by Wahl [11]. (Right) The average neutron multiplicity per fission as a function of the heavy fragment mass from this study compared to data from Refs. [20, 22]. The dashed red line indicates the mean multiplicity per fission.

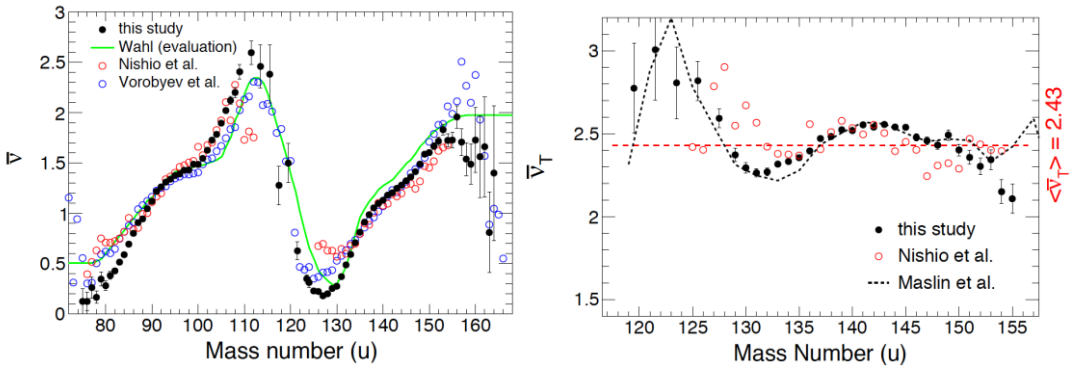

Figure 9. (Left) The average neutron multiplicity per fission as a function of the TKE, result from this study is compared to experimental data from Refs.[20–22, 24]. The black line represents a straight line with an inverse slope of 12.0 MeV/n, obtained from a least square fit of the data from this study. (Right) The fission yields as a function of TKE from the different studies are compared.

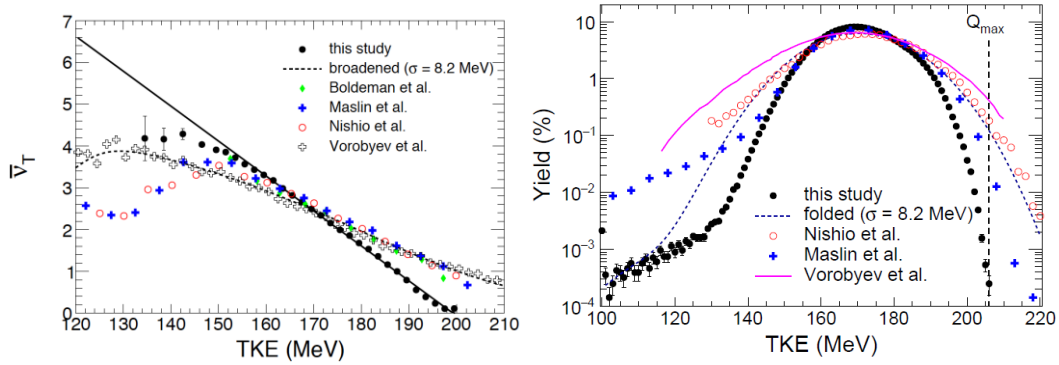

On the left hand side of **Figure 9** the average neutron multiplicity per fission is plotted as a function of the fragment TKE. As expected, a close to linear dependence is observed, except for at low TKE. A least square fit, indicated by the full black line, results in $\partial \mathrm{TKE}/\partial\bar{\nu}$ = 12.0 MeV/n. This value is substantially lower than the values 16.7-18.5 MeV/n reported in earlier studies, performed at thermal incident neutron energies (Maslin et al., 1967, Boldeman et al., 1971, Nishio et al., 1998 and Vorobyev et al., 2010). This inverse slope is closely related to the energy cost to emit a neutron, although it should not be directly interpreted as this quantity (Nifenecker, 1973). It is not expected that the small increase in the excitation energy of the compound nucleus compared to thermal neutron induced fission would have an influence on the energy cost to emit a neutron. Hence, we propose a different interpretation, which is purely of instrumental nature. On the right hand side of **Figure 9** the fission fragment TKE distribution from the present measurement is compared to the data of (Nishio et al., 1998, Maslin et al., 1967 and

Vorobyev et al., 2010). The distributions from these earlier experiments appear broadened. Substantial amounts of yields are found above the maximum available energy, as determined by the Q-value for the fragmentation where the heavy fragment is the doubly magic ^{132}Sn nucleus. Since the TKE cannot physically exceed the maximum available energy, the TKE distributions from these earlier studies must suffer from substantial resolution broadening. The dashed lines in **Figure 9** represent the result of folding the data from this study with a Gaussian resolution function in order to reproduce the TKE distribution of Nishio et al. If the same broadening is applied when determining $\bar{\nu}(\mathrm{TKE})$ qualitatively features in the literature data are reproduced, i.e. a reduction in slope and $\bar{\nu}$ different from zero at the maximum available energy. There are discrepancies at low TKE where the data of Nishio et al. (1998) and Maslin et al. (1967) show a strong decrease in $\bar{\nu}$ that cannot be explained by the resolution broadening. Examining the TKE distributions tailings at low energies can be observed. Events belonging to this tailing are likely due to scattering of the fission fragments in the target-foil and/or surrounding materials, as already noted by Maslin et al (1967). The neutron emission from such energy degraded fission events is expected to be close to the average value. This is consistent with the observed decrease in $\bar{\nu}$ at lower TKE as the tailing become more and more dominant in the yield. The tailing is present also in the data from this study, although at much lower intensities compared to the data of Nishio et al. (1998) and Maslin et al. (1967). Due to the presence of the tailing we must conclude that the decrease in slope of $\bar{\nu}$ below TKE of 140 MeV is not of a physical origin. A comparison of the experimental result for average neutron multiplicity per fission with different model calculations, taken from a recent review of the available fission fragment de-excitation models (Capote et al., 2016 and Schmidt et al., 2016), is shown in **Figure 10**. The different models presented by Capote et al. (2016) agree well with each other. Therefore, not all of them are included in the figure. It is clear that the model calculations are in much better agreement with the present data set than with earlier experiments.

Figure 10. The average neutron multiplicity per fission as a function of the TKE, experimental results from this study is compared to model calculations from three different fission fragment deexcitation models.

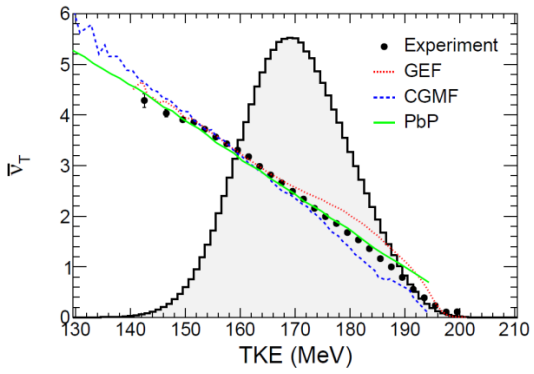

4.2.3 Prompt neutron energy

The neutron energy in the c.m. frame η has also been evaluated on an event-by-event basis. The integral spectrum is presented as a ratio to a Maxwellian with a fitted temperature of 0.826 MeV in **Figure 11**. The average neutron energy as a function of the fission fragment mass is compared to theoretical calculations and an earlier experiment in **Figure 12**. The average values for the light- and heavy fragment groups are 1.23 MeV and 1.26 MeV, respectively. The average c.m. neutron energy is an important validation parameter for neutron emission models as it relates to both the

excitation energy partition between the fragments as well as the distribution of temperatures in the sequential emission of neutrons. The quantity is also important for application as it has a direct influence on the laboratory neutron spectrum. It is evident from **Figure 12** that $\bar{\eta}(A)$ is almost symmetric with respect to symmetric mass division, in contrast to $\bar{\nu}(A)$ which shows the well know sawtooth shape. This result is very similar to earlier findings for the prompt fission neutrons from ^{252}Cf(sf) (Göök et al., 2014, Budtz-Jørgensen and Knitter). The different model predictions are in general in good agreement with the experimental data. The FREYA model does however predict a pronounced sawtooth shape which is not observed in the experiment. All models predict a more or less pronounced minimum in the region below A=130, while the experimental data shows only a flattening of the trend when approaching this region from heavier masses. Considering the strong slope of the mass yield curve and the experimental mass resolution it is expected that sharp changes in the properties of neutrons as a function of mass are washed out.

Figure 11. The prompt neutron spectrum in the c.m. frame, integrated over all fragmentations, presented as a ratio to a Maxwellian with temperature 0.826 MeV..

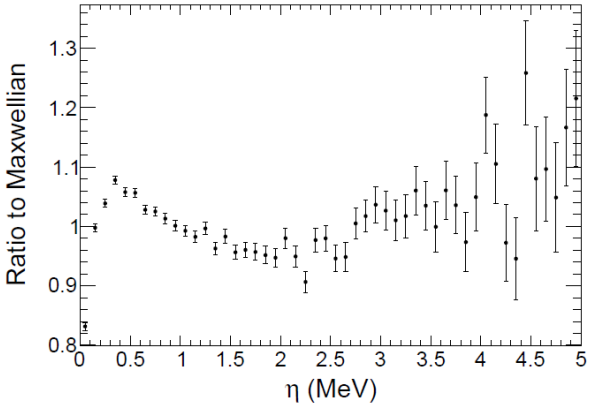

Figure 12. The average c.m. neutron energy $\bar{\eta}$ as a function of the fission fragment mass, results from this experiment are compared to model predictions from CGMF and PbP (Capote et al., 2016) and experimental data from Nishio et al. (1998).

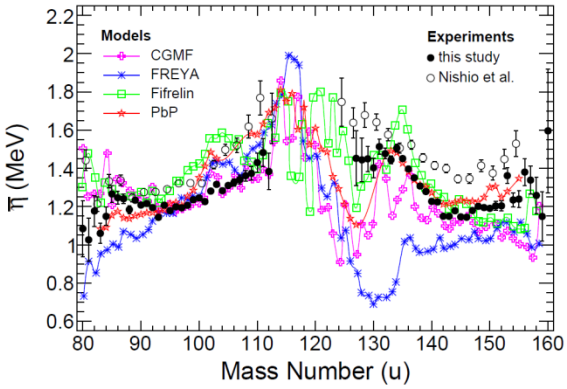

5 Experimental Results in the resonance region

The energies of the incident neutrons which induce fission have been determined via their flight time. In **Figure 13** the incident neutron energy spectrum for the range below 40 eV is shown. From this spectrum one can clearly see the individually resolved resonances. Selection by setting a narrow gate around a particular resonance allows us to study the properties of that resonance.

Figure 13. Selected range of the incident neutron energy spectrum, as determined from the time-of-flight to the fission chamber. Three of the strongest resonances are labelled with their respective energies.

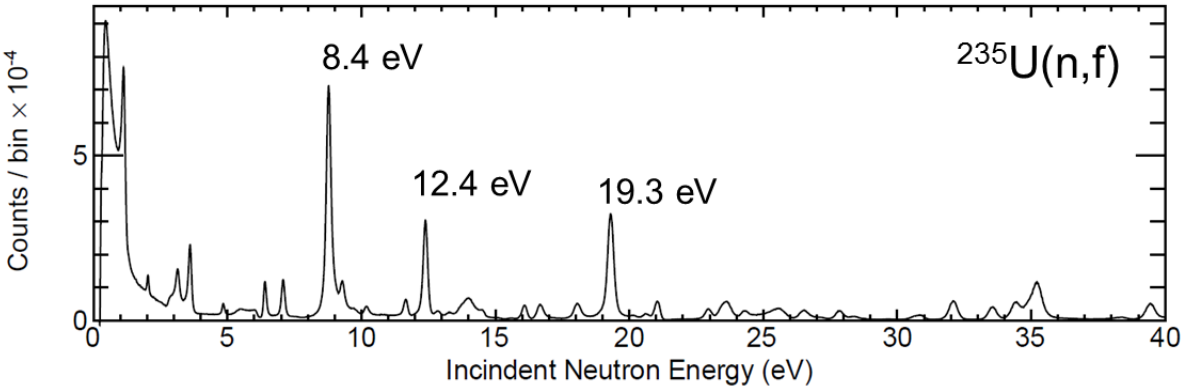

In **Figure 14** the relative $\bar{\nu}$ determined in this study for individual resonance gates is compared to data from the literature (Howe et al., 1976 and Reed, 1973). One may recognize that the relative $\bar{\nu}$ exhibits structure as a function of the incident neutron energy. In fact, a statistical test of the assumption of a constant $\bar{\nu}$ for resolved resonances bellow 40 eV gives χ^2 = 47.4 for 30 degrees of freedom. This value suggests that the assumption should be rejected with better than 80% confidence. The conjecture of structure in $\bar{\nu}$ is further supported by a positive linear correlation factor ρ = 0.48±0.18 between the results of the present study and those of Howe et al. (1976).

Figure 14. Relative resonance $\bar{\nu}$ as a function of the incident neutron energy.

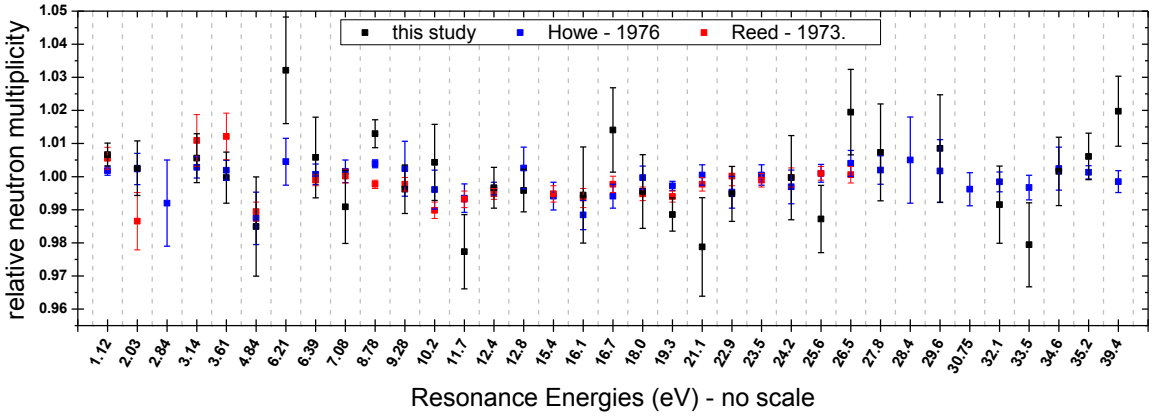

In order to better understand the origins of the fluctuating $\bar{\nu}$ we have studied the properties of the fission fragments in the resonance region. In **Figure 15** the average TKE of the fission fragments for the same resonance gates as in **Figure 14** is plotted. Compared to earlier studies at Gelina (Hambsch, 1987), the present result show clear

improvements in statistical accuracy. It is clear that changes in the average TKE from resonance to resonance is present, a change in incident neutron energy of only a few eV can change the TKE by several hundred keV. The dramatic changes in the TKE are caused by changes in the fragment mass yield. As an example of this, the difference in mass yield compared to thermal neutron induced fission for the 19.3 eV resonance and the 1.12 eV resonance is shown in **Figure 16**. The 19.3 eV resonance, which shows a large increase in TKE, shows an increased mass yield in the region around mass 130. On the other hand, the 1.12 eV resonance shows no significant change in either the TKE or the mass yield. Due to the difference in available energy for different mass regions, the increase in fission fragment mass yield around mass 130 will lead to an increase in the average TKE. Hence, the change in mass yield is apparently responsible for change in the average TKE. In order to quantitatively show that this applies for all resonances, the correlation between the change in average TKE and mean heavy fragment mass compared to thermal neutron induced fission is shown in **Figure 17**.

Figure 15. Change in the average TKE of fission fragments for selected resonance gates compared to thermal neutron induced fission.

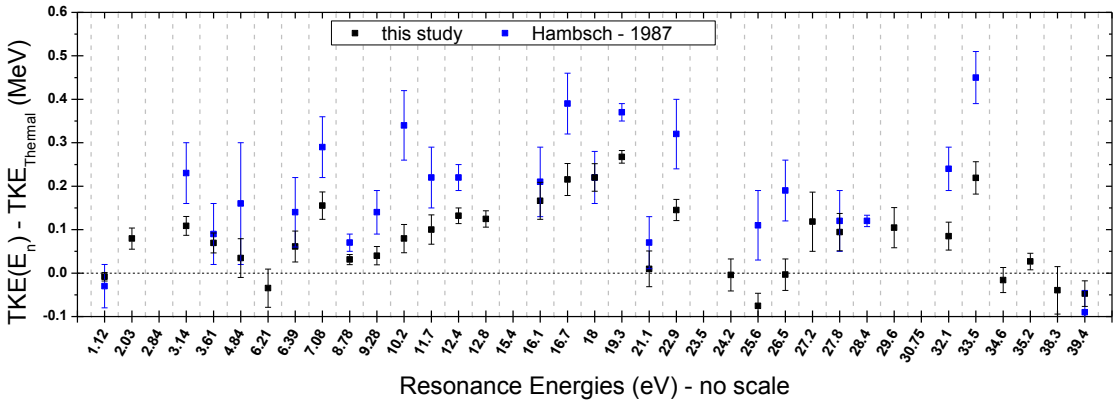

Figure 16. Change in the fragment mass yield for two selected resonance gates compared to thermal neutron induced fission.

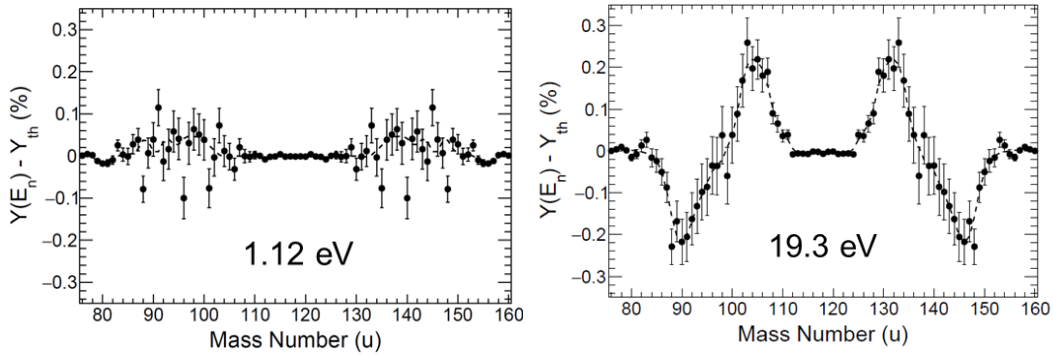

Figure 17. Correlation between observed change in average TKE and average heavy fragment mass compared to thermal neutron induced fission. Each point corresponds to a resonance or resonance group.

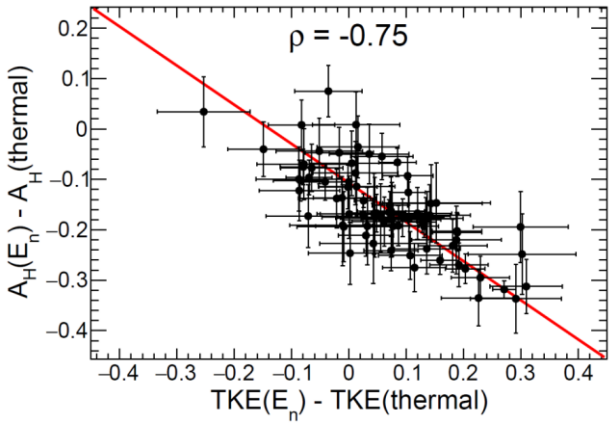

It is expected that the observed changes in the fragment mass yield will affect also the neutron multiplicities, due to the observed correlations between these observables. This assertion is verified by data in **Figure 18**, showing a correlation plot between average heavy-fragment mass and $\bar{\nu}$ as well as average TKE and $\bar{\nu}$. In order to make the comparison meaningful only resonances for which a relative statistical uncertainty better than 1 % could be achived.is shown in the figure.

Figure 18. Correlation between observed change in average TKE as well as average heavy fragment mass with the observed neutron multiplicity, for resonance gates where a relative statistical uncertainty better than 1 % was achieved.

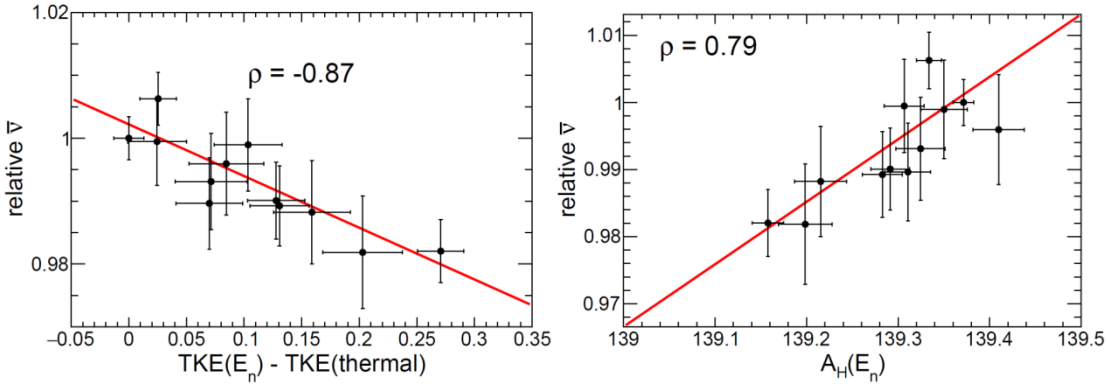

6 Conclusions

A multi-parameter experiment on correlations between the properties of fission fragments and PFNs in the reaction ^{235}U(n,f) has been presented.

The laboratory angular distribution of prompt neutrons has been compared with a model calculation based on isotropic emission from fully accelerated fragments. The model agrees fairly well with the experimental data, however the model calculation does underestimate the neutron yield at large angles with the fission axis. The underestimation amounts to 2.5 % of the total neutron yield.

Results on average neutron multiplicities in correlation with fission fragment mass and TKE show significant differences to earlier studies on this reaction, induced by thermal neutrons. The sawtooth shape of the average neutron multiplicity per fragment show more pronounced minima at mass 130 and 80 u. The TKE dependence of the neutron multiplicity per fission shows an inverse slope approximately 35\% weaker than observed in earlier studies (Maslin et al., 1967, Boldeman et al., 1971, Nishio et al., 1998, Vorobyev et al., 2010). The difference can be attributed to improved fission fragment TKE resolution in the present experiment. The present result for the average neutron multiplicity as a function of TKE is in good agreement with model calculations (Capote et al., 2016 , Schmidt et al., 2016).

Fluctuations in neutron multiplicity as a function of incident neutron energy have been observed. The fluctuations show clear correlation with fluctuations observed in the fission fragment mass yield.

References

Boldeman, J.W., de L. Musgrove, A.R., Walsh, R. L., Aust. J. Phys. 24, 821 (1971)

Bowman, H.R., Thompson, S.G., Milton, J.C.D., Swiatecki, W.J., Phys. Rev. 126, 2120 (1962)

Budtz-Jørgensen, C. , Knitter, H.H., Nucl. Phys. A 490, 307 (1988)

Capote, R., Chen, Y.-J., Hambsch, F.-J., Kornilov, N.V., Lestone, J.P., Litaize, O., Morillon, B., Neudecker, D., Oberstedt, S., Ohsawa, T., Otuka, N., Pronyaev, V.G., Saxena, A., Serot, O., Shcherbakov, O.A., Shu, N.-C., Smith, D.L. , Talou, P. Trkov, A. , Tudora, A.C., Vogt, R., Vorobyev, A.S., Nucl. Data Sheets 131, 1 (2016)

De Saint Jean (Coord.), C., McKnight, R. D., (Monitor), "Co-ordinated Evaluation of Plutonium-239 in the Resonance Region", Report NEA/NSC/WPEC/DOC(2014)447, Nuclear Energy Agency, OECD, Paris, France (2014).

Eismont, V.P., Jour. Nucl. Energy A/B 20, 875 (1965)

Gavron, A., Nucl. Instr. and Meth. 115, 99 (1974)

Geltenbort, P., Gönnenwein, F., Oed, A., Radiation Effects 93, 57 (1986)

Göök, A. , Geerts, W., Hambsch, F.-J., Oberstedt, S., Vidali, M., Zeynalov, S., Nucl. Instr. and Meth.A 830, 366 (2016)

Göök, A., Hambsch, F.-J., Oberstedt, S., EPJ Web of Conf. ND 2016 Int. Conf. on Nucl. Data for Sci. and Tech. (2016)

Göök, A. , Hambsch, F.-J., Vidali, M., Phys. Rev. C 90, 064611 (2014)

Howe, R.E., Phillips, T.W., Bowman, C.D., Phys. Rev. C 13, 13 (1976)

Kornilov, N.V., Hambsch, F.-J., Vorobyev, A.S., Nucl. Phys. A 789, 55 (2007)

Kornilov, N.V. Tech. rep., IAEA, INDC(USA)-108 (2015)

Kornilov, N.V., Fabry, I., Oberstedt, S., Hambsch, F.-J., Nucl. Instr. and Meth. A 599, 226 (2009)

Kornilov, N.V., Hambsch, F.-J., Fabry, I., Oberstedt, S., Belgya, T., Kis, Z., Szentmiklosi, L., Simakov., S., Nucl. Sci. and Eng. 165, 117 (2010)

Lemaire, S., Talou, P., Kawano, T., Chadwick, M., Madland, D., Phys. Rev. C 72 (2005)

Mannhart, W., IAEA-TECDOC-410 (Leningrad, 1986), p. 158

Maslin, E.E., Rodgers, A.L., W.G.F. Core, Phys. Rev. 164, 1520 (1967)

Nifenecker, H. , Signarbieux, C., Babinet, R., Poitou, J., 3rd IAEA Symp. on the Physics and Chemistry of Fission 2, 117 (1973)

Nishio, K., Nakagome, Y., Yamamoto, H., Kimura, I., Nucl. Phys. A 632, 540 (1998)

Peneliau, Y., Litaize, O., Archier, P. De Saint Jean, C. "^{239}Pu Prompt Fission Neutron Spectra Impact on a Set of Criticality and Experimental Reactor Benchmarks", *Nucl. Data Sheets* 118, 459–462 (2014).

Rizea, M., Carjan, N., Nucl. Phys. A 909, 50 (2013)

Schmidt, K.H., Jurado, B., Amouroux, C., Schmitt, C. Nucl. Data Sheets 131, 107 (2016)

Tajik, M. , Ghal-Eh, N., Etaati, G.R., Afarideh, H., Nucl. Instr. and Meth. A 704, 104 (2013)

Terrell, J., Phys. Rev. 127, 880 (1962)

Trkov, A., Capote, R., Pronyaev, V.G., Nucl. Data Sheets 123, 8 (2015)

Verbinski, V.V., Burrus, W.R., Love, T.A., Zobel, W., Hill, N.W., Textor, R., Nucl. Instr. and Meth. 65, 8 (1968)

Vorobyev, A.S., Shcherbakov, O., Gagarski, A., Val'ski, G., Petrov, G., EPJ Web of Conf. 8, 03004 (2010)

Vorobyev, A.S., Shcherbakov, O.A., Pleva, Yu.S., Gagarski, A.M, Val'ski, G.V., Petrov, G.A., Petrova, V.I., Zavarukhina, T.A. Nucl. Instr. and Meth. A 598, 795 (2009)

Wahl, C., Atomic Data and Nuclear Data Tables 39, 56 (1988)

List of abbreviations and definitions

PFN	Prompt fission neutron
PFNS	Prompt fission neutron spectrum
$\bar{\nu}$	Prompt fission neutron multiplicity
IC	Ionization chamber
TKE	Total kinetic energy
2E	Double kinetic energy
c.m.	Centre of mass

List of figures

GETTING IN TOUCH WITH THE EU

In person

All over the European Union there are hundreds of Europe Direct information centres. You can find the address of the centre nearest you at: http://europea.eu/contact

On the phone or by email

Europe Direct is a service that answers your questions about the European Union. You can contact this service:

- by freephone: 00 800 6 7 8 9 10 11 (certain operators may charge for these calls),

- at the following standard number: +32 22999696, or

- by electronic mail via: http://europa.eu/contact

FINDING INFORMATION ABOUT THE EU

Online

Information about the European Union in all the official languages of the EU is available on the Europa website at: http://europa.eu

EU publications
You can download or order free and priced EU publications from EU Bookshop at: http://bookshop.europa.eu. Multiple copies of free publications may be obtained by contacting Europe Direct or your local information centre (see http://europa.eu/contact).

KJ-NA-28840-EN-N

JRC Mission

As the science and knowledge service of the European Commission, the Joint Research Centre's mission is to support EU policies with independent evidence throughout the whole policy cycle.

EU Science Hub
ec.europa.eu/jrc

@EU_ScienceHub

EU Science Hub - Joint Research Centre

Joint Research Centre

EU Science Hub

Publications Office

doi:10.2760/481835

ISBN 978-92-79-74380-1